Florida Institute of Technology

Scholarship Repository @ Florida Tech

Aerospace, Physics, and Space Science Faculty Publications

Department of Aerospace, Physics, and Space Sciences

2013

Azimuthal Anisotropy Of π^0 And η Mesons In Au + Au Collisions At $\sqrt{s_{NN}}$=200

Andrew Marshall Adare

Gyöngyi Baksay

László A. Baksay

Marcus Hohlmann

Follow this and additional works at: https://repository.fit.edu/apss_faculty

 Part of the Astrophysics and Astronomy Commons

Azimuthal anisotropy of π^0 and η mesons in Au + Au collisions at $\sqrt{s_{NN}} = 200$ GeV

A. Adare,[13] S. Afanasiev,[30] C. Aidala,[43,44] N. N. Ajitanand,[62] Y. Akiba,[56,57] H. Al-Bataineh,[50] J. Alexander,[62] K. Aoki,[35,56] Y. Aramaki,[12] E. T. Atomssa,[36] R. Averbeck,[63] T. C. Awes,[52] B. Azmoun,[7] V. Babintsev,[24] M. Bai,[6] G. Baksay,[20] L. Baksay,[20] K. N. Barish,[8] B. Bassalleck,[49] A. T. Basye,[1] S. Bathe,[5,8] V. Baublis,[55] C. Baumann,[45] A. Bazilevsky,[7] S. Belikov,[7,*] R. Belmont,[67] R. Bennett,[63] A. Berdnikov,[59] Y. Berdnikov,[59] A. A. Bickley,[13] J. S. Bok,[71] K. Boyle,[63] M. L. Brooks,[39] H. Buesching,[7] V. Bumazhnov,[24] G. Bunce,[7,57] S. Butsyk,[39] C. M. Camacho,[39] S. Campbell,[63] C.-H. Chen,[63] C. Y. Chi,[14] M. Chiu,[7] I. J. Choi,[71] R. K. Choudhury,[4] P. Christiansen,[41] T. Chujo,[66] P. Chung,[62] O. Chvala,[8] V. Cianciolo,[52] Z. Citron,[63] B. A. Cole,[14] M. Connors,[63] P. Constantin,[39] M. Csanád,[18] T. Csörgő,[70] T. Dahms,[63] S. Dairaku,[35,56] I. Danchev,[67] K. Das,[21] A. Datta,[43] G. David,[7] A. Denisov,[24] A. Deshpande,[57,63] E. J. Desmond,[7] O. Dietzsch,[60] A. Dion,[63] M. Donadelli,[60] O. Drapier,[36] A. Drees,[63] K. A. Drees,[6] J. M. Durham,[39,63] A. Durum,[24] D. Dutta,[4] S. Edwards,[21] Y. V. Efremenko,[52] F. Ellinghaus,[13] T. Engelmore,[14] A. Enokizono,[38] H. En'yo,[56,57] S. Esumi,[66] B. Fadem,[46] D. E. Fields,[49] M. Finger,[9] M. Finger, Jr.,[9] F. Fleuret,[36] S. L. Fokin,[34] Z. Fraenkel,[69,*] J. E. Frantz,[51,63] A. Franz,[7] A. D. Frawley,[21] K. Fujiwara,[56] Y. Fukao,[56] T. Fusayasu,[48] I. Garishvili,[64] A. Glenn,[13] H. Gong,[63] M. Gonin,[36] Y. Goto,[56,57] R. Granier de Cassagnac,[36] N. Grau,[2,14] S. V. Greene,[67] M. Grosse Perdekamp,[25,57] T. Gunji,[12] H.-Å. Gustafsson,[41,*] J. S. Haggerty,[7] K. I. Hahn,[19] H. Hamagaki,[12] J. Hamblen,[64] R. Han,[54] J. Hanks,[14] E. P. Hartouni,[38] E. Haslum,[41] R. Hayano,[12] X. He,[22] M. Heffner,[38] T. K. Hemmick,[63] T. Hester,[8] J. C. Hill,[28] M. Hohlmann,[20] W. Holzmann,[14] K. Homma,[23] B. Hong,[33] T. Horaguchi,[23] D. Hornback,[64] S. Huang,[67] T. Ichihara,[56,57] R. Ichimiya,[56] J. Ide,[46] Y. Ikeda,[66] K. Imai,[29,35,56] M. Inaba,[66] D. Isenhower,[1] M. Ishihara,[56] T. Isobe,[12,56] M. Issah,[67] A. Isupov,[30] D. Ivanischev,[55] B. V. Jacak,[63] J. Jia,[7,62] J. Jin,[14] B. M. Johnson,[7] K. S. Joo,[47] D. Jouan,[53] D. S. Jumper,[1] F. Kajihara,[12] S. Kametani,[56] N. Kamihara,[57] J. Kamin,[63] J. H. Kang,[71] J. Kapustinsky,[39] K. Karatsu,[35,56] D. Kawall,[43,57] M. Kawashima,[56,58] A. V. Kazantsev,[34] T. Kempel,[28] A. Khanzadeev,[55] K. M. Kijima,[23] B. I. Kim,[33] D. H. Kim,[47] D. J. Kim,[31] E. Kim,[61] E.-J. Kim,[10] S. H. Kim,[71] Y.-J. Kim,[25] E. Kinney,[13] K. Kiriluk,[13] Á. Kiss,[18] E. Kistenev,[7] L. Kochenda,[55] B. Komkov,[55] M. Konno,[66] J. Koster,[25] D. Kotchetkov,[49] A. Kozlov,[69] A. Král,[15] A. Kravitz,[14] G. J. Kunde,[39] K. Kurita,[56,58] M. Kurosawa,[56] Y. Kwon,[71] G. S. Kyle,[50] R. Lacey,[62] Y. S. Lai,[14] J. G. Lajoie,[28] A. Lebedev,[28] D. M. Lee,[39] J. Lee,[19] K. Lee,[61] K. B. Lee,[33] K. S. Lee,[33] M. J. Leitch,[39] M. A. L. Leite,[60] E. Leitner,[67] B. Lenzi,[60] X. Li,[11] P. Liebing,[57] L. A. Linden Levy,[13] T. Liška,[15] A. Litvinenko,[30] H. Liu,[39,50] M. X. Liu,[39] B. Love,[67] R. Luechtenborg,[45] D. Lynch,[7] C. F. Maguire,[67] Y. I. Makdisi,[6] A. Malakhov,[30] M. D. Malik,[49] V. I. Manko,[34] E. Mannel,[14] Y. Mao,[54,56] H. Masui,[66] F. Matathias,[14] M. McCumber,[63] P. L. McGaughey,[39] N. Means,[63] B. Meredith,[25] Y. Miake,[66] A. C. Mignerey,[42] P. Mikeš,[9,27] K. Miki,[56,66] A. Milov,[7] M. Mishra,[3] J. T. Mitchell,[7] A. K. Mohanty,[4] Y. Morino,[12] A. Morreale,[8] D. P. Morrison,[7,†] T. V. Moukhanova,[34] J. Murata,[56,58] S. Nagamiya,[32] J. L. Nagle,[13,‡] M. Naglis,[69] M. I. Nagy,[18] I. Nakagawa,[56,57] Y. Nakamiya,[23] T. Nakamura,[32] K. Nakano,[56,65] J. Newby,[38] M. Nguyen,[63] R. Nouicer,[7] A. S. Nyanin,[34] E. O'Brien,[7] S. X. Oda,[12] C. A. Ogilvie,[28] M. Oka,[66] K. Okada,[57] Y. Onuki,[56] A. Oskarsson,[41] M. Ouchida,[23,56] K. Ozawa,[12] R. Pak,[7] V. Pantuev,[26,63] V. Papavassiliou,[50] I. H. Park,[19] J. Park,[61] S. K. Park,[33] W. J. Park,[33] S. F. Pate,[50] H. Pei,[28] J.-C. Peng,[25] H. Pereira,[16] V. Peresedov,[30] D. Yu. Peressounko,[34] C. Pinkenburg,[7] R. P. Pisani,[7] M. Proissl,[63] M. L. Purschke,[7] A. K. Purwar,[39] H. Qu,[22] J. Rak,[31] A. Rakotozafindrabe,[36] I. Ravinovich,[69] K. F. Read,[52,64] K. Reygers,[45] V. Riabov,[55] Y. Riabov,[55] E. Richardson,[42] D. Roach,[67] G. Roche,[40] S. D. Rolnick,[8] M. Rosati,[28] C. A. Rosen,[13] S. S. E. Rosendahl,[41] P. Rosnet,[40] P. Rukoyatkin,[30] P. Ružička,[27] B. Sahlmueller,[45,63] N. Saito,[32] T. Sakaguchi,[7] K. Sakashita,[56,65] V. Samsonov,[55] S. Sano,[12,68] T. Sato,[66] S. Sawada,[32] K. Sedgwick,[8] J. Seele,[13] R. Seidl,[25] A. Yu. Semenov,[28] R. Seto,[8] D. Sharma,[69] I. Shein,[24] T.-A. Shibata,[56,65] K. Shigaki,[23] M. Shimomura,[66] K. Shoji,[35,56] P. Shukla,[4] A. Sickles,[7] C. L. Silva,[60] D. Silvermyr,[52] C. Silvestre,[16] K. S. Sim,[33] B. K. Singh,[3] C. P. Singh,[3] V. Singh,[3] M. Slunečka,[9] R. A. Soltz,[38] W. E. Sondheim,[39] S. P. Sorensen,[64] I. V. Sourikova,[7] N. A. Sparks,[1] P. W. Stankus,[52] E. Stenlund,[41] S. P. Stoll,[7] T. Sugitate,[23] A. Sukhanov,[7] J. Sziklai,[70] E. M. Takagui,[60] A. Taketani,[56,57] R. Tanabe,[66] Y. Tanaka,[48] K. Tanida,[35,56,57] M. J. Tannenbaum,[7] S. Tarafdar,[3] A. Taranenko,[62] P. Tarján,[17] H. Themann,[63] T. L. Thomas,[49] M. Togawa,[35,56] A. Toia,[63] L. Tomášek,[27] H. Torii,[23] R. S. Towell,[1] I. Tserruya,[69] Y. Tsuchimoto,[23] C. Vale,[7,28] H. Valle,[67] H. W. van Hecke,[39] E. Vazquez-Zambrano,[14] A. Veicht,[25] J. Velkovska,[67] R. Vértesi,[17,70] A. A. Vinogradov,[34] M. Virius,[15] V. Vrba,[27] E. Vznuzdaev,[55] X. R. Wang,[50] D. Watanabe,[23] K. Watanabe,[66] Y. Watanabe,[56,57] F. Wei,[28] R. Wei,[62] J. Wessels,[45] S. N. White,[7] D. Winter,[14] J. P. Wood,[1] C. L. Woody,[7] R. M. Wright,[1] M. Wysocki,[13] W. Xie,[57] Y. L. Yamaguchi,[12] K. Yamaura,[23] R. Yang,[25] A. Yanovich,[24] J. Ying,[22] S. Yokkaichi,[56,57] Z. You,[54] G. R. Young,[52] I. Younus,[37,49] I. E. Yushmanov,[34] W. A. Zajc,[14] C. Zhang,[52] S. Zhou,[11] and L. Zolin[30]

(PHENIX Collaboration)

[1]*Abilene Christian University, Abilene, Texas 79699, USA*

[2]*Department of Physics, Augustana College, Sioux Falls, South Dakota 57197, USA*

[3]*Department of Physics, Banaras Hindu University, Varanasi 221 005, India*

[4]*Bhabha Atomic Research Centre, Bombay 400 085, India*

[5]*Baruch College, City University of New York, New York, New York, 10010 USA*

[6]*Collider-Accelerator Department, Brookhaven National Laboratory, Upton, New York 11973-5000, USA*

[7]*Physics Department, Brookhaven National Laboratory, Upton, New York 11973-5000, USA*

[8]*University of California - Riverside, Riverside, California 92521, USA*

[9]*Charles University, Ovocný trh 5, Praha 1, 116 36, Prague, Czech Republic*

 ©2013 American Physical Society

[10]*Chonbuk National University, Jeonju, 561-756, Korea*
[11]*Science and Technology on Nuclear Data Laboratory, China Institute of Atomic Energy, Beijing 102413, People's Republic of China*
[12]*Center for Nuclear Study, Graduate School of Science, University of Tokyo, 7-3-1 Hongo, Bunkyo, Tokyo 113-0033, Japan*
[13]*University of Colorado, Boulder, Colorado 80309, USA*
[14]*Columbia University, New York, New York 10027 and Nevis Laboratories, Irvington, New York 10533, USA*
[15]*Czech Technical University, Zikova 4, 166 36 Prague 6, Czech Republic*
[16]*Dapnia, CEA Saclay, F-91191, Gif-sur-Yvette, France*
[17]*Debrecen University, H-4010 Debrecen, Egyetem tér 1, Hungary*
[18]*ELTE, Eötvös Loránd University, H-1117 Budapest, Pázmány P.s. 1/A, Hungary*
[19]*Ewha Womans University, Seoul 120-750, Korea*
[20]*Florida Institute of Technology, Melbourne, Florida 32901, USA*
[21]*Florida State University, Tallahassee, Florida 32306, USA*
[22]*Georgia State University, Atlanta, Georgia 30303, USA*
[23]*Hiroshima University, Kagamiyama, Higashi-Hiroshima 739-8526, Japan*
[24]*IHEP Protvino, State Research Center of Russian Federation, Institute for High Energy Physics, Protvino, 142281, Russia*
[25]*University of Illinois at Urbana-Champaign, Urbana, Illinois 61801, USA*
[26]*Institute for Nuclear Research of the Russian Academy of Sciences, prospekt 60-letiya Oktyabrya 7a, Moscow 117312, Russia*
[27]*Institute of Physics, Academy of Sciences of the Czech Republic, Na Slovance 2, 182 21 Prague 8, Czech Republic*
[28]*Iowa State University, Ames, Iowa 50011, USA*
[29]*Advanced Science Research Center, Japan Atomic Energy Agency, 2-4 Shirakata Shirane, Tokai-mura, Naka-gun, Ibaraki-ken 319-1195, Japan*
[30]*Joint Institute for Nuclear Research, 141980 Dubna, Moscow Region, Russia*
[31]*Helsinki Institute of Physics and University of Jyväskylä, P.O. Box 35, FI-40014 Jyväskylä, Finland*
[32]*KEK, High Energy Accelerator Research Organization, Tsukuba, Ibaraki 305-0801, Japan*
[33]*Korea University, Seoul, 136-701, Korea*
[34]*Russian Research Center "Kurchatov Institute", Moscow, 123098 Russia*
[35]*Kyoto University, Kyoto 606-8502, Japan*
[36]*Laboratoire Leprince-Ringuet, Ecole Polytechnique, CNRS-IN2P3, Route de Saclay, F-91128, Palaiseau, France*
[37]*Physics Department, Lahore University of Management Sciences, Lahore, Pakistan*
[38]*Lawrence Livermore National Laboratory, Livermore, California 94550, USA*
[39]*Los Alamos National Laboratory, Los Alamos, New Mexico 87545, USA*
[40]*LPC, Université Blaise Pascal, CNRS-IN2P3, Clermont-Fd, 63177 Aubiere Cedex, France*
[41]*Department of Physics, Lund University, Box 118, SE-221 00 Lund, Sweden*
[42]*University of Maryland, College Park, Maryland 20742, USA*
[43]*Department of Physics, University of Massachusetts, Amherst, Massachusetts 01003-9337, USA*
[44]*Department of Physics, University of Michigan, Ann Arbor, Michigan 48109-1040, USA*
[45]*Institut fur Kernphysik, University of Muenster, D-48149 Muenster, Germany*
[46]*Muhlenberg College, Allentown, Pennsylvania 18104-5586, USA*
[47]*Myongji University, Yongin, Kyonggido 449-728, Korea*
[48]*Nagasaki Institute of Applied Science, Nagasaki-shi, Nagasaki 851-0193, Japan*
[49]*University of New Mexico, Albuquerque, New Mexico 87131, USA*
[50]*New Mexico State University, Las Cruces, New Mexico 88003, USA*
[51]*Department of Physics and Astronomy, Ohio University, Athens, Ohio 45701, USA*
[52]*Oak Ridge National Laboratory, Oak Ridge, Tennessee 37831, USA*
[53]*IPN-Orsay, Universite Paris Sud, CNRS-IN2P3, BP1, F-91406, Orsay, France*
[54]*Peking University, Beijing 100871, People's Republic of China*
[55]*PNPI, Petersburg Nuclear Physics Institute, Gatchina, Leningrad region, 188300, Russia*
[56]*RIKEN Nishina Center for Accelerator-Based Science, Wako, Saitama 351-0198, Japan*
[57]*RIKEN BNL Research Center, Brookhaven National Laboratory, Upton, New York 11973-5000, USA*
[58]*Physics Department, Rikkyo University, 3-34-1 Nishi-Ikebukuro, Toshima, Tokyo 171-8501, Japan*
[59]*Saint Petersburg State Polytechnic University, St. Petersburg, 195251 Russia*
[60]*Universidade de São Paulo, Instituto de Física, Caixa Postal 66318, São Paulo CEP05315-970, Brazil*
[61]*Seoul National University, Seoul, Korea*
[62]*Chemistry Department, Stony Brook University, SUNY, Stony Brook, New York 11794-3400, USA*
[63]*Department of Physics and Astronomy, Stony Brook University, SUNY, Stony Brook, New York 11794-3400, USA*
[64]*University of Tennessee, Knoxville, Tennessee 37996, USA*
[65]*Department of Physics, Tokyo Institute of Technology, Oh-okayama, Meguro, Tokyo 152-8551, Japan*
[66]*Institute of Physics, University of Tsukuba, Tsukuba, Ibaraki 305, Japan*
[67]*Vanderbilt University, Nashville, Tennessee 37235, USA*

[68]*Waseda University, Advanced Research Institute for Science and Engineering, 17 Kikui-cho, Shinjuku-ku, Tokyo 162-0044, Japan*
[69]*Weizmann Institute, Rehovot 76100, Israel*
[70]*Institute for Particle and Nuclear Physics, Wigner Research Centre for Physics, Hungarian Academy of Sciences (Wigner RCP, RMKI), H-1525 Budapest 114, P.O. Box 49, Budapest, Hungary*
[71]*Yonsei University, IPAP, Seoul 120-749, Korea*
(Received 18 September 2013; published 20 December 2013)

The azimuthal anisotropy coefficients v_2 and v_4 of π^0 and η mesons are measured in Au + Au collisions at $\sqrt{s_{NN}} = 200$ GeV as a function of transverse momentum p_T (1–14 GeV/c) and centrality. The extracted v_2 coefficients are found to be consistent between the two meson species over the measured p_T range. The ratio of v_4/v_2^2 for π^0 mesons is found to be independent of p_T for 1–9 GeV/c, implying a lack of sensitivity of the ratio to the change of underlying physics with p_T. Furthermore, the ratio of v_4/v_2^2 is systematically larger in central collisions, which may reflect the combined effects of fluctuations in the initial collision geometry and finite viscosity in the evolving medium.

DOI: 10.1103/PhysRevC.88.064910 PACS number(s): 25.75.Dw

I. INTRODUCTION

A novel form of nuclear matter, where quarks and gluons are deconfined yet interact strongly with each other, is produced in heavy ion collisions at the Relativistic Heavy Ion Collider (RHIC) [1–4] and the Large Hadron Collider (LHC) [5]. The hydrodynamic expansion of this matter, as well as its interactions with hard scattered partons, result in the anisotropic emission of hadrons [6,7]. Measurements of azimuthal anisotropy for particle production provide valuable information on the transport properties of the matter [8–10].

The magnitude of the anisotropy can be studied from the azimuthal angle (ϕ) distribution of particles relative to the second-order[1] event plane (EP) angle (Φ) accumulated over many events [11,12]:

$$\frac{dN}{d\Delta\phi} \propto 1 + 2\sum_{k=1}^{\infty} v_{2k}\cos(2k\Delta\phi), \tag{1}$$

where $\Delta\phi = (\phi - \Phi)$ and v_{2k} are even-order Fourier coefficients, which generally are nonzero around the elliptic flow EP [11]. In the *event plane* method, an estimated EP angle Ψ is determined from the particles in the event. Due to the finite number of particles used to determine Ψ, the Ψ angle is an approximation of the true EP angle Φ. The coefficient v_{2k} is measured by correlating particles with Ψ to obtain the raw values $v_{2k}^{\rm obs} = \langle\cos(2k[\phi - \Psi])\rangle$, which are then corrected by a resolution factor (Res$\{2k\Psi\}$) that accounts for the spread of Ψ about Φ [11]:

$$v_{2k} = \frac{v_{2k}^{\rm obs}}{\text{Res}\{2k\Psi\}} = \frac{\langle\cos(2k[\phi - \Psi])\rangle}{\langle\cos(2k[\Psi - \Phi])\rangle}, \quad k = 1,2. \tag{2}$$

To minimize the nonflow biases from dijets, the particles used to estimate Ψ are selected in a pseudorapidity range that is well separated (typically one unit or more) from the particles used to evaluate $v_{2k}^{\rm obs}$ [13].

Recently, experiments at RHIC and LHC have measured significant v_{2k} values for $k = 1$–3 for various particle species and over a broad range in p_T [14–18]. For particles with low transverse momenta ($p_T \lesssim 3$ GeV/c), the coefficients are understood in terms of pressure-driven *flow* in an initial "almond-shaped" collision zone produced in noncentral collisions [19]. For higher transverse momenta ($p_T \gtrsim 6$–10 GeV/c), the anisotropy reflected by the v_{2k} coefficients can be attributed to jet quenching [20]—the process by which hard scattered partons interact and lose energy in the hot and dense medium prior to fragmenting into hadrons. This energy loss manifests as a suppression of hadron yields [21], which depends on the average path length that partons propagate through the medium [22,23], and v_2 for example stems from the fact that the partons traveling in a direction parallel to the Φ angle are less suppressed than those traveling in the direction perpendicular to the Φ angle [7].

The present work exploits various PHENIX detector subsystems with a broad range in pseudorapidity for the EP determination, and provides detailed differential measurements of v_2 and v_4 for π^0 mesons and v_2 for η mesons in $\sqrt{s_{NN}} = 200$ GeV Au + Au collisions. The v_2 and v_4 measurements for π^0 mesons extend our earlier work [22,23]. The v_2 measurements for η mesons probe the particle species dependence of jet quenching and test the consistency of the data with medium-induced partonic energy loss prior to vacuum hadronization [17,24]. In this vacuum hadronization picture, high-p_T π^0 and η mesons are thought to arise from fragmentation of energetic partons after they lose energy in the medium, and hence the two types of mesons are expected to show similar level of suppression [25] and similar path-length dependence or v_2. Furthermore, this analysis provides a test of the previous observed scaling relation between v_2 and v_4, i.e., the observation that the v_4/v_2^2 ratio is approximately independent of p_T [14–16,26]. This analysis also allows a detailed study of the biases from dijets in the determination of the event plane.

*Deceased.
†PHENIX Co-Spokesperson: morrison@bnl.gov
‡PHENIX Co-Spokesperson: jamie.nagle@colorado.edu

[1]The v_4 coefficient can be measured with respect to the second-order event plane or the fourth-order event plane. In the analysis presented in this work, all v_4 coefficients are measured with respect to the second-order event plane.

II. MEASUREMENT

A. Data set and centrality

The measurements are based on a Au + Au collision data set at $\sqrt{s_{NN}} = 200$ GeV collected during the 2007 running period. The minimum bias events are selected by the beam-beam counters (BBCs). The collision vertex along the beam direction, z, is measured by the BBCs. After an offline vertex cut of $|z| < 30$ cm and run quality selections, a total of $\sim 3.5 \times 10^9$ minimum bias events are obtained. Event centrality for these events are determined by the number of charged particles detected in the BBCs [13]. A Glauber model Monte Carlo simulation [27] that includes the responses of the BBCs is used to estimate, for each centrality selection, the average number of participating nucleons $N_{\rm part}$.

B. Event plane measurement

The EP angle is estimated using several detectors installed symmetrically on both sides of the nominal collision point along the beamline: the BBCs [28], the muon piston calorimeters (MPCs) [29], and the reaction-plane detectors (RXNs) [30]. The BBCs comprise two sets of 64 Čerenkov counter modules, located at $z = \pm 144$ cm from the nominal collision point, and measure the number of charged particles over the pseudorapidity region $3.1 < |\eta| < 3.9$. Each MPC is equipped with $PbWO_4$ crystal scintillator towers. The north MPC has 220 towers spanning $3.1 < \eta < 3.9$, while the south MPC has 196 towers spanning $-3.7 < \eta < -3.1$. The MPCs have almost the same azimuth and η coverage as the BBCs, but have finer granularity and detect both charged and neutral particles, and hence have better EP resolution. The RXNs are situated at $z = \pm 40$ cm from the nominal interaction point. Each comprises 12 azimuthally segmented scintillator paddles with photomultiplier readout. They are covered with a 2 cm (3.6 radiation length) thick lead photon converter and are sensitive to both charged particles and photons. The RXNs cover the pseudorapidity region $1.0 < |\eta| < 2.8$. They are further subdivided into an outer part ($\rm RXN_{out}$, $1.0 < |\eta| < 1.5$) and an inner part ($\rm RXN_{in}$, $1.5 < |\eta| < 2.8$).

Table I outlines the η acceptance of BBCs, MPCs, and RXNs, as well as several combined detectors from which the EP are estimated. These combinations allow for a reliable estimate of the systematic uncertainties in this measurement. The results reported in this paper use the EP from MPC + $\rm RXN_{in}$ [22], which provides very good resolution and minimizes the possible nonflow biases from jets and dijets [13].

TABLE I. Summary of the η coverage for the detector combinations used for the event plane measurements.

Detectors	η range
BBC	$\pm[3.1,3.9]$
MPC	$[-3.7,-3.1]$, $[3.1,3.9]$
$\rm RXN_{in}$	$\pm[1.5,2.8]$
$\rm RXN_{out}$	$\pm[1.0,1.5]$
RXN(in + out)	$\pm[1.0,2.8]$
MPC + $\rm RXN_{in}$	$\pm[1.5,2.8]$, $[-3.7,-3.1]$, $[3.1,3.9]$

The resolution factor $\rm Res\{2k\Psi\}$ is determined using the two subevents (2SE) and three subevents (3SE) methods [11], as outlined in our previous analyses [15,24]. In the 2SE method, the signal of a given detector combination in Table I is divided into two subevents covering equal pseudorapidity ranges in opposite hemispheres. The resolution of each subevent is calculated directly from the correlation between the two subevents:

$$\rm Res\{2k\Psi^A\} = Res\{2k\Psi^B\} = \sqrt{\langle \cos(2k[\Psi^A - \Psi^B])\rangle}. \quad (3)$$

The resolution can be expressed analytically as

$$\rm Res\{2k\Psi\} = \langle \cos(2k\Delta\Psi)\rangle = \frac{\chi\sqrt{\pi}}{2} e^{-\frac{\chi^2}{2}} \left[I_{\frac{k-1}{2}}\left(\frac{\chi^2}{2}\right) + I_{\frac{k+1}{2}}\left(\frac{\chi^2}{2}\right)\right], \quad (4)$$

where I_α are modified Bessel functions of the first kind, and the resolution parameter $\chi \propto \sqrt{M}$ is related to the multiplicity M. The resolution parameter of the full detector is determined as $\chi = \sqrt{2}\chi_{\rm A} = \sqrt{2}\chi_{\rm B}$, which is then used to determine $\rm Res\{2k\Psi\}$ via Eq. (4).

The 3SE method determines the resolution factor of a given detector from the correlations of its EP with those for two other detectors in different pseudorapidity ranges:

$$\rm Res\{2k\Psi^A\} = \sqrt{\frac{\langle \cos(2k[\Psi^A - \Psi^B])\rangle \langle \cos(2k[\Psi^A - \Psi^C])\rangle}{\langle \cos(2k[\Psi^B - \Psi^C])\rangle}}. \quad (5)$$

The main advantage of the 3SE method is that, for a given detector A, there are many choices of detectors B and C which provide independent estimates of the resolution of A. The differences between the resolution estimates for the 2SE and 3SE methods are included in the evaluation of systematic uncertainties.

The left panel of Fig. 1 summarizes the $N_{\rm part}$ dependence of the 2SE resolution factors for various detector combinations as indicated. The resolution factors peak around $N_{\rm part} \sim 180$ (i.e., the 20%–30% centrality bin) with maximum values of 0.75 for RXN, 0.53 for MPC, and 0.4 for the BBC. The resolution factors for $\rm RXN_{in}$ and $\rm RXN_{out}$ are similar and show a

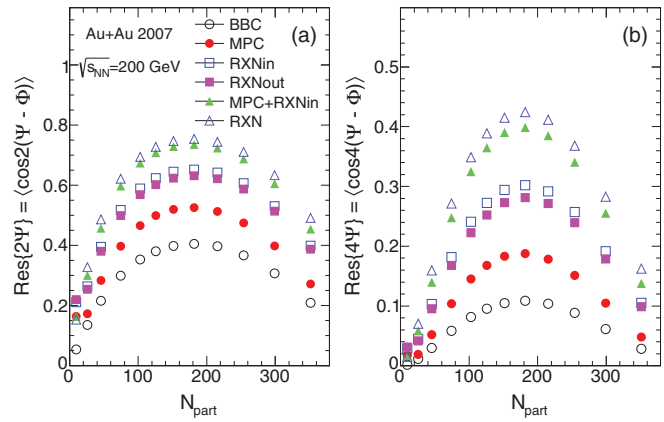

FIG. 1. (Color online) Resolutions for v_2 (left) and v_4 (right) calculated using various detectors for event plane.

maximum of ∼0.65. The resolution factors for MPC + RXN_{in} are very close to those for the full RXN. The right panel of Fig. 1 shows resolution factors for v_4 that are much smaller than those for v_2. The associated resolution factors also peak for $N_{\text{part}} \sim 180$, reaching maximum values of 0.45, 0.18, 0.1, and 0.4 for the full RXN, MPC, BBC, and MPC + RXN_{in} respectively.

C. Measurements of π^0 and η meson anisotropy

1. Reconstruction of π^0 and η mesons

Neutral pion and η mesons are measured via their $\gamma\gamma$ decay channel in the electromagnetic calorimeter (EMCal, $|\eta| < 0.35$) [31]. The EMCal comprises the lead-scintillator and lead-glass subdetectors, covering 0.75π and 0.25π in azimuth, respectively. Photons are identified using various cuts on the shower shape observed in the EMCal, as well as by comparing the observed shapes to a template profile function measured from test beam data. The invariant mass $m_{\gamma\gamma}$ is calculated for photon pairs, which pass an energy asymmetry cut $\alpha = |E_1 - E_2|/(E_1 + E_2) < 0.8$ and have a minimum separation of 8 cm between their impact points in the EMCal. The combinatorial background distribution in $m_{\gamma\gamma}$ is estimated with the event mixing technique where the two photons are selected from different events satisfying similar global requirements such as vertex, centrality, and event plane direction. The mixed-event $m_{\gamma\gamma}$ distributions are then normalized in the sidebands of the π^0 and η peaks in the real event distributions and are subtracted. A small residual background is parameterized by a first-order polynomial in the regions below and above the π^0 and η peak, and then subtracted from the $m_{\gamma\gamma}$ distribution. The raw π^0 and η meson yields are calculated by integrating a $\pm 2\sigma$ window in $m_{\gamma\gamma}$ around their respective peaks. This window is varied ($\pm 2\sigma$ vs $\pm 3\sigma$) to check the stability of the yield. The ratios of signal to background (S/N) for π^0 and η mesons varies strongly with p_T and centrality. The S/N value generally increases with p_T and increases from central to peripheral collisions. The values of S/N for π^0 and η mesons are given in Table II for events in 0%–20% collisions. In this analysis, the reconstruction of the π^0 and η mesons is limited to $p_T > 1$ GeV/c and $p_T > 3$ GeV/c respectively, where the yields of the two mesons can be extracted with relatively small uncertainty. Further details can be found in Ref. [23,32].

2. The $dN/d\Delta\phi$ method

The first method for the extraction of v_2 and v_4 follows the analysis method outlined in our prior work [28]. The photon pairs in each p_T and centrality bin are divided according to their angle relative to the estimated EP angle, $\Delta\phi = \phi - \Psi$, into six bins in the interval of $[0,\pi/2]$. The yields of π^0 and η mesons are extracted independently in each bin and then parameterized by

$$\frac{dN}{d\Delta\phi} = N_0\left[1 + 2v_2^{\text{obs}}\cos(2\Delta\phi) + 2v_4^{\text{obs}}\cos(4\Delta\phi)\right] \quad (6)$$

to obtain v_{2k}^{obs}. The values of v_{2k}^{obs} are also calculated directly via a discrete Fourier transform:

$$v_{2k}^{\text{obs}} = \frac{\sum_{i=1}^{6} N_i \cos(2k\Delta\phi_i)}{\sum_{i=1}^{6} N_i}, \quad (7)$$

where the N_i stands for the yield in the ith angular bin. The two results are found to be consistent within 2% of their central values. Because of the finite bin width in $\Delta\phi$, the extracted v_{2k}^{obs} values need to be corrected up by a smearing factor $\sigma_k = \frac{k\delta}{\sin(k\delta)}$, which accounts for the finite bin width $\delta = \pi/12$.

The v_2 and v_4 values for this method are obtained by applying both the resolution correction [Eq. (2)] and smearing correction to v_2^{obs} and v_4^{obs} for each centrality and p_T selection. To check the sensitivity of the yield extraction on our choices of bin width in $\Delta\phi$, the v_2 and v_4 values are also calculated using 18 bins in $\Delta\phi$ for $p_T < 10$ GeV/c. The results are found to be consistent with the 6 bin results within 3% of the average of the two measurements.

3. Invariant mass method

The second method of extracting v_2 and v_4 for π^0 mesons follows the procedure outlined in Refs. [33–35]. In this method, the anisotropy of same-event or foreground (frg) pairs and mixed-events or background (bkg) pairs are determined as a function of $m_{\gamma\gamma}$, denoted as $v_{2k}^{\text{frg}}(m_{\gamma\gamma})$ and $v_{2k}^{\text{bkg}}(m_{\gamma\gamma})$, respectively. The anisotropy of foreground pairs can be expressed as the sum of the contributions from the signal pairs (sig) and the background pairs in each $m_{\gamma\gamma}$ bin:

$$N_{\text{frg}}\, v_{2k}^{\text{frg}} = N_{\text{sig}}\, v_{2k}^{\text{sig}} + N_{\text{bkg}}\, v_{2k}^{\text{bkg}}, \quad (8)$$

$$N_{\text{frg}} = N_{\text{sig}} + N_{\text{bkg}}\ , \quad (9)$$

which gives the expression

$$v_{2k}^{\text{sig}}(m_{\gamma\gamma}) = \frac{v_{2k}^{\text{frg}}(m_{\gamma\gamma}) - v_{2k}^{\text{bkg}}(m_{\gamma\gamma})[1 - R(m_{\gamma\gamma})]}{R(m_{\gamma\gamma})}, \quad (10)$$

where $R = N_{\text{sig}}/(N_{\text{sig}} + N_{\text{bkg}})$ is the fraction of the total number of pairs comprising the signal.

Figure 2 illustrates the steps in calculating $v_{2k}^{\text{sig}}(m_{\gamma\gamma})$ for a given p_T and centrality bin. Figure 2(a) shows the distributions of the foreground $N_{\text{frg}}(m_{\gamma\gamma})$, total background $N_{\text{bkg}}(m_{\gamma\gamma})$, and the extracted signal $N_{\text{sig}}(m_{\gamma\gamma})$. The N_{bkg} is determined from mixed events in concert with a linear parametrization of the residual background, as described earlier. Figure 2(b) shows the resulting $R(m_{\gamma\gamma})$. The signal anisotropy coefficients are calculated directly as $v_{2k}^{\text{sig}} = \langle\cos[2k(\phi - \Psi)]\rangle$ as a function of $m_{\gamma\gamma}$, as shown by the open circles in Figs. 2(c) and 2(d). They have a concave shape in the π^0 signal region, and show a minimum at the π^0 mass peak. In regions far away from the

TABLE II. The ratios of signal to background (S/N) for π^0 and η mesons at several p_T in 0%–20% most central collisions. The values are given for pairs integrated in a $\pm 2\sigma$ window in $m_{\gamma\gamma}$ around their respective peaks.

p_T (GeV/c)	1	3	6	10
π^0 S/N	0.01	0.15	2	8
η S/N	N/A	0.01	0.1	1

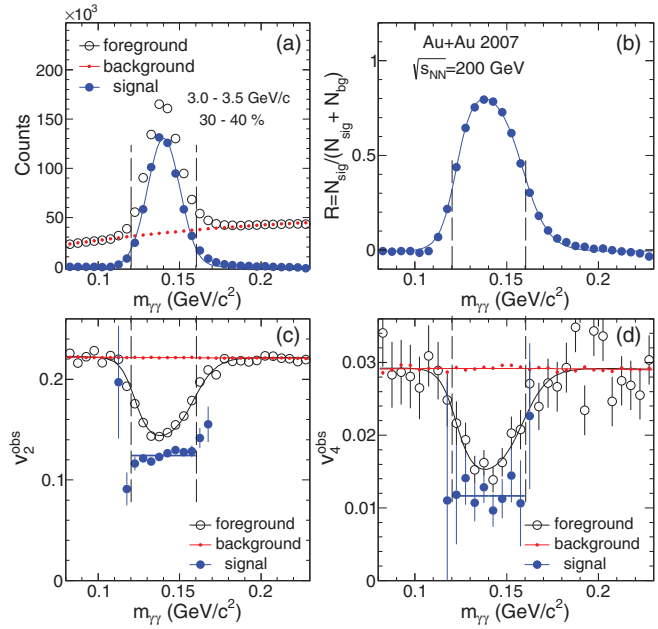

FIG. 2. (Color online) The $m_{\gamma\gamma}$ distributions used to obtain $v_2^{\rm obs}$ and $v_4^{\rm obs}$ values. (a) Distributions of foreground $N_{\rm frg}$, background $N_{\rm bkg}$, and signal $N_{\rm sig}$, (b) the signal fraction $R = N_{\rm sig}/(N_{\rm sig} + N_{\rm bkg})$, (c) the $v_2^{\rm obs}$ distributions for foreground, background and signal, and (d) the $v_4^{\rm obs}$ distributions for foreground, background, and signal. The vertical dashed lines indicate the two-standard-deviation window around the π^0 peak.

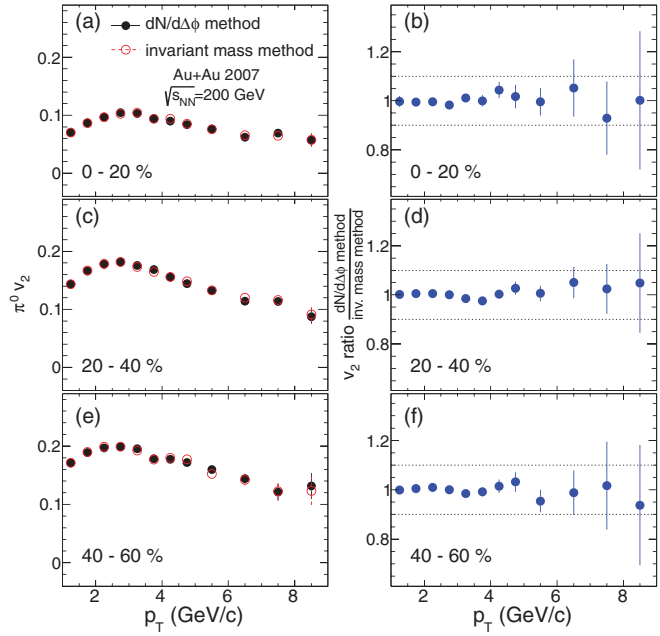

FIG. 3. (Color online) Comparison of π^0 v_2 for the $dN/d\Delta\phi$ and the invariant mass methods of analysis for several centrality selections (left panels). The corresponding ratios are shown in the right panels, with the dashed curves indicating a $\pm 10\%$ deviation from unity.

π^0 mass, the $v_{2k}^{\rm sig}$ values vary slowly with $m_{\gamma\gamma}$, reflecting the anisotropy of the background. The concave shape is a general feature of the invariant mass method for reconstructing v_2 of decay particles [33–35]: the background photon pairs on average have a small opening angle owing to the asymmetry cut, and hence they have a larger anisotropy compared to photons from π^0 decay.

The two photons of the mixed-event pairs are chosen from an event class with similar event plane orientations, so they have a sizable anisotropy $v_{2k}^{\rm bg,mix}(m_{\gamma\gamma})$. However, because the two events used to construct the mixed event do not have exactly the same EP angle, $v_{2k}^{\rm bg,mix}(m_{\gamma\gamma})$ is smaller than the $v_{2k}^{\rm bkg}(m_{\gamma\gamma})$ by a factor that depends on the EP resolution and the bin width of the EP class used for event mixing, but is independent of $m_{\gamma\gamma}$. Hence the $v_{2k}^{\rm bkg}(m_{\gamma\gamma})$ value is obtained by first scaling the measured $v_{2k}^{\rm bg,mix}(m_{\gamma\gamma})$ distribution to match the $v_{2k}^{\rm frg}(m_{\gamma\gamma})$ in regions three standard deviations away from the π^0 peak. The resulting $v_{2k}^{\rm bkg}(m_{\gamma\gamma})$ distributions are indicated by the small dotted symbols in Figs. 2(c) and 2(d). The anisotropy coefficients of the signals $v_{2k}^{\rm sig}$ are then calculated bin by bin in $m_{\gamma\gamma}$ according to Eq. (10). They are shown by the solid symbols in Figs. 2(c) and 2(d).

Figure 2(c) shows a slight increase of $v_2^{\rm sig}$ at the upper end of the π^0 peak. This increase is due to overlapping clusters, which also manifests as an excess in the Gaussian fit to the signal Figs. 2(a). Since the $v_2^{\rm sig}$ measurement is dominated by the points in the vicinity of the π^0 peak, the influence of this increase on $v_2^{\rm sig}$ is less than 3% of its magnitude and it is included in the systematic uncertainties.

Figures 3 and 4 compare the v_2 and v_4 values obtained from the two analysis methods. The v_2 values agree within the

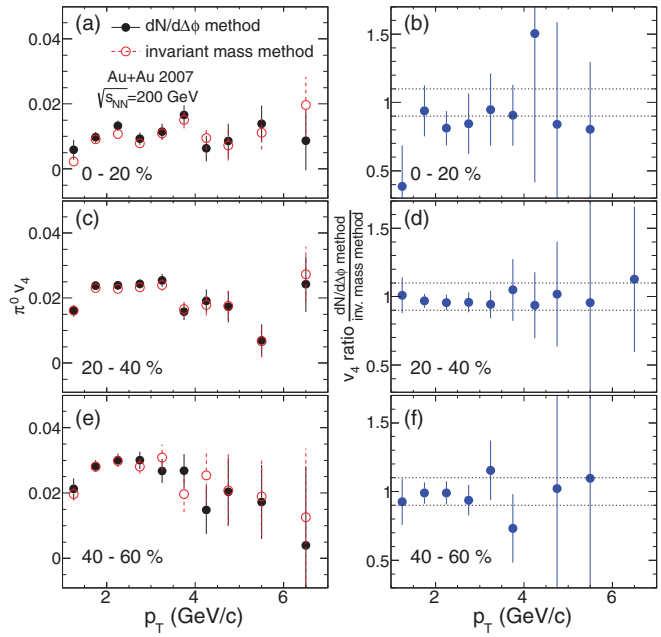

FIG. 4. (Color online) Comparison of π^0 v_4 for the $dN/d\Delta\phi$ and the invariant mass methods of analysis for several centrality selections (left panels). The corresponding ratios are shown in the right panels, with the dashed curves indicating a $\pm 10\%$ deviation from unity.

statistical uncertainties; the systematic deviation is less than 3%. The v_4 from the $dN/d\Delta\phi$ method is systematically larger by about 5%–10%. This is due to small residual backgrounds in the integration window in the $dN/d\Delta\phi$ method. This background also leads to larger statistical uncertainty for the $dN/d\Delta\phi$ method, because it is evaluated separately for each angular bin, while in reality this background is correlated between these angular bins. The $dN/d\Delta\phi$ method also has an extra source of systematic uncertainty arising from the number of $\Delta\phi$ bins, which can become significant for v_4. Consequently, the invariant mass method is used to generate the v_4 and v_4/v_2^2 results. As a cross-check, the π^0 v_2 and v_4 results are also compared and found to be consistent with the results for identified charged pions from Ref. [15].

4. *Evaluating the jet bias*

This measurement assumes that the EP determination is not strongly biased by the selection of π^0 and η mesons at midrapidity. At high p_T, such a bias could stem from dijets associated with the π^0 or η mesons. The pseudorapidity spread of particles from jets containing the π^0 or η meson is typically much smaller than the pseudorapidity gap between the EP and the EMCal. However, the large rapidity swing of the away-side jet could bring jet-associated particles into the detectors used to calculate the EP, leading to a potential bias of the v_2 and v_4 values.

In earlier studies of high-momentum particles, PHENIX has estimated the magnitude of this bias by embedding PYTHIA dijet events into HIJING events modulated with the experimentally measured v_2 signal [13,36]. The away-side jet was found to bias the EP determination and, hence, the v_{2k} signal at high p_T, depended on the pseudorapidity gap. In general the bias is expected to decrease with increasing pseudorapidity gap, and should be smallest for EP determined by the MPC pseudorapidity range. In this analysis, our ability to measure the EP in different pseudorapidity ranges allows for a data-driven quantification of the pseudorapidity dependence of the jet bias, as discussed below.

Figure 5 shows the EP resolution of various detectors for events containing a high-p_T π^0 ($p_T > 5$ GeV/c). No systematic p_T dependence is observed for the selections studied. Figure 6 compares the $v_2(p_T)$ values for π^0, obtained with event planes determined in the MPC ($3 < |\eta| < 4$), $\mathrm{RXN_{in}}$ ($1.5 < |\eta| < 2.8$), and $\mathrm{RXN_{out}}$ ($1 < |\eta| < 1.5$). At low p_T ($\lesssim$5 GeV/c), the v_2 values obtained from these event planes are comparable in more central collisions. For higher p_T, they deviate from each other, with larger v_2 for $\mathrm{RXN_{out}}$ and smaller v_2 for the MPC. For peripheral collisions, the values obtained with $\mathrm{RXN_{out}}$ are significantly higher over the full p_T range. These trends are consistent with the presence of a dijet bias, which grows as the pseudorapidity gap between the EP and the π^0 or η meson is reduced. For pseudorapidity gaps $\lesssim$1–1.5, the dijets bias the EP angle towards the direction of the π^0, which results in a larger v_2 value. Apparently, this bias does not affect the resolution corrections. In summary, for the centrality range used in this analysis (0%–60%), the use of MPC + $\mathrm{RXN_{in}}$ is sufficient to suppress the effects of this jet bias to within the statistical uncertainty of the measurement (see also Ref. [22]).

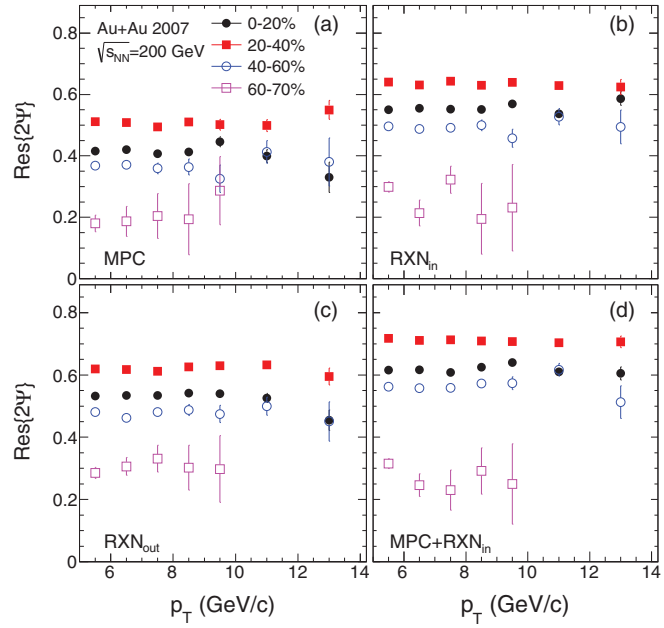

FIG. 5. (Color online) Event plane resolution Res{2Ψ} for events containing a high-p_T π^0. Results are plotted as a function of p_T of the π^0 for several EP detectors in several centrality ranges.

5. *Systematic uncertainties*

The primary results of this analysis are obtained with the MPC + $\mathrm{RXN_{in}}$ event plane. The uncertainties in the resolution factors for this event plane are obtained by comparing the values obtained for the 2SE and the 3SE methods. They are estimated to be 8% (12%) in central collisions and 4% (6%) in midcentral collisions for Res{2Ψ} (Res{4Ψ}). These uncertainties allow all points to move up and down by the same multiplicative factor.

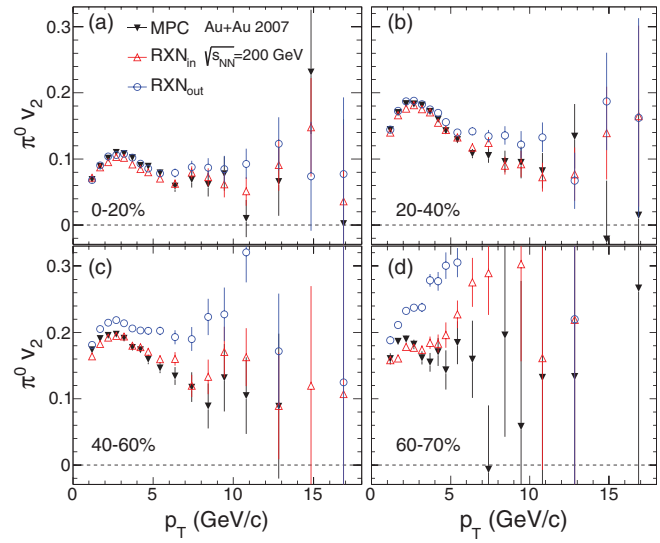

FIG. 6. (Color online) Comparison of v_2 vs p_T for π^0 mesons obtained at several centralities with event planes determined by detectors in different pseudorapidity ranges.

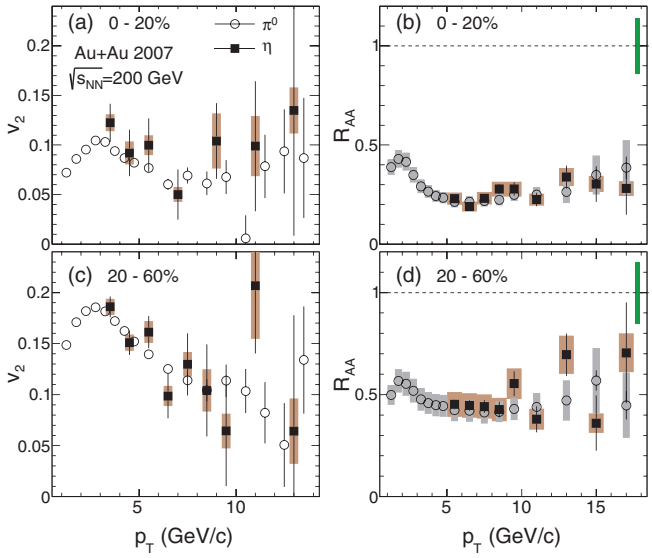

FIG. 7. (Color online) The v_2 (left panels) and nuclear modification factor $R_{\rm AA}$ (right panels) for π^0 and η mesons in 0%–20% (top panels) and 20%–60% (bottom panels) centrality ranges. The v_2 results for π^0 mesons are identical to what was published in Ref. [22]. The $R_{\rm AA}$ data are taken from Ref. [37] (π^0, $p_T < 5$ GeV/c), Ref. [23] (π^0, $p_T > 5$ GeV/c), and Ref. [32] (η meson). The uncertainties of $R_{\rm AA}$ associated with $N_{\rm coll}$ and normalization are common between π^0 and η mesons, and are shown as shaded boxes around unity.

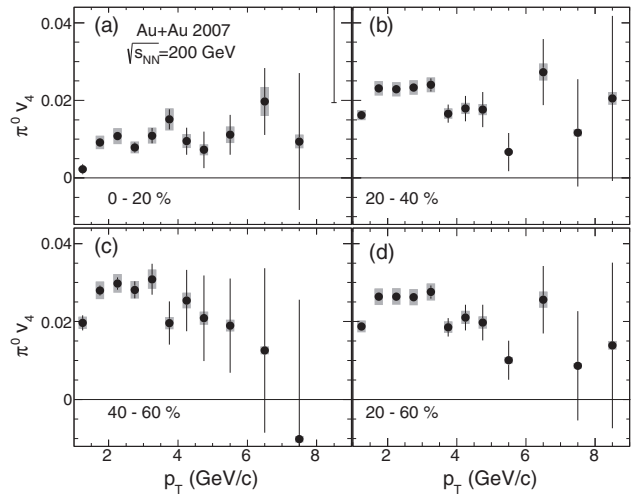

FIG. 8. The v_4 coefficient vs p_T for π^0 mesons for the indicated centrality selections. The shaded boxes represent the systematic uncertainties.

The systematic uncertainties for $v_2^{\rm obs}$ and $v_4^{\rm obs}$ are estimated by varying the identification cuts for π^0 and η mesons, the parametrization of the residual background and the peak integration window in the $m_{\gamma\gamma}$ distributions. These uncertainties are correlated in p_T and are added in quadrature to give the total systematic uncertainties. For the π^0 analysis, these uncertainties are estimated to be 10% (15%) in central collisions and 3% (5%) in midcentral collisions for $v_2^{\rm obs}$ ($v_4^{\rm obs}$). For the η-meson analysis, the uncertainties are significantly larger primarily because of the lower signal-to-background ratio. These uncertainties are estimated to be 15% in central collisions and ∼10% at other centralities.

III. RESULTS AND DISCUSSION

The primary results of this analysis are obtained with MPC + $\rm RXN_{in}$ event plane. The left panels of Fig. 7 compare the v_2 for π^0 and η mesons for $p_T \gtrsim 4$ GeV/c, both obtained with the $dN/d\Delta\phi$ method for two centrality ranges. Within uncertainties, the magnitude of the v_2 values for both particle species are the same for the measured p_T range. This agreement indicates that the differences between their masses [$m_\eta = 0.548$ GeV, $m_{\pi^0} = 0.135$ GeV] and quark content [$(u\bar{u} - d\bar{d})/\sqrt{2}$ for π^0 and $(u\bar{u} + d\bar{d} - 2s\bar{s})/\sqrt{6}$ for η in the SU(3) limit] do not lead to appreciable differences in the π^0- and η-meson v_2 values for the centrality ranges studied. A clear decrease of v_2 with p_T is also evident, especially for the 20%–60% centrality selection. These patterns complement our earlier suppression measurements [23,32] (reproduced in the right panel of Fig. 7), which show the same suppression patterns for π^0 and η mesons. These results are in agreement with the expectations for in-medium energy loss of parent partons prior to their fragmentation into hadrons in the p_T region where jet quenching is expected to be dominant mechanism ($p_T \gtrsim 4$–5 GeV/c).

The transition from anisotropy driven by hydrodynamic flow to anisotropy driven by jet quenching can be probed by the ratio v_4/v_2^2. Perfect fluid hydrodynamics predicts a value of 0.5 for this ratio [38]. However, geometrical fluctuations and other dynamical fluctuations, as well as viscous damping, can significantly increase the magnitude of this ratio, especially in central collisions [26,39]. Furthermore, the directions that maximize collective flow and jet quenching may not be the same [40,41]. Hence, this ratio could change in the p_T region where jet quenching begins to dominate.

The results of $v_4(p_T)$ and the v_4/v_2^2 ratio for π^0 in several centrality ranges are shown in Figs. 8 and 9, respectively. Results are also combined into a wide centrality range (20%–60%) for better statistical precision. Figure 8 shows that significant v_4 values are observed even for $p_T > 5$ GeV/c. The v_4/v_2^2 ratios shown in Fig. 9 are approximately independent of p_T, with values of ∼1.0 and ∼0.8 for the 0%–20% and the 20%–40% and 40%–60% centrality selections respectively. This pattern at low p_T ($p_T \lesssim 5$ GeV/c) is consistent with our prior observations of this ratio for inclusive charged hadron measurements [15]. On the other hand, possible variations of this ratio at higher p_T could be masked, owing to the limited statistics of this measurement. The deviation of the v_4/v_2^2 value from the expectation of ideal hydrodynamics and the increase of this ratio from midcentral to more central collisions may reflect the combined effects of fluctuations in the initial geometry and finite viscosity in the evolving medium [39].

IV. SUMMARY AND CONCLUSIONS

PHENIX has measured the azimuthal anisotropy for π^0 and η mesons in Au + Au collisions at $\sqrt{s_{NN}} = 200$ GeV.

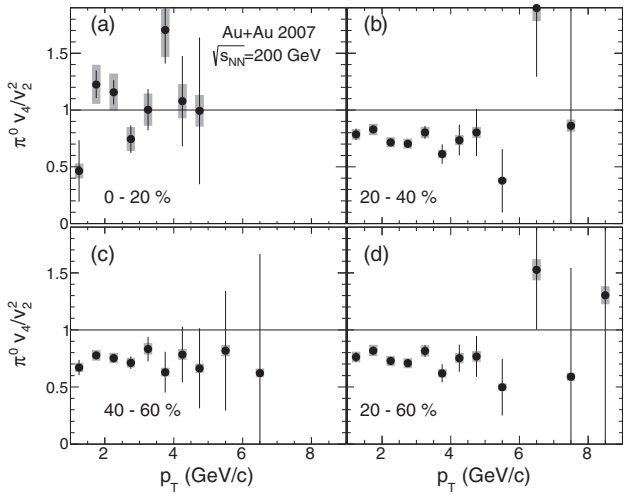

FIG. 9. The ratio v_4/v_2^2 vs p_T for π^0 mesons for the indicated centrality selections. The shaded boxes represent the systematic uncertainties.

The anisotropy coefficients v_2 and v_4 are measured with event planes determined in forward detectors, which enable a minimum pseudorapidity gap of 1.2 units between the event plane and the π^0 or η mesons. This pseudorapidity gap is found to greatly reduce autocorrelation biases due to dijets over the 0%–60% centrality range. The magnitudes of the v_2 values extracted for π^0 and η mesons, over the common p_T range of 3–14 GeV/c, are observed to be similar, suggesting in-medium energy loss of parent partons prior to their fragmentation into hadrons. The v_4 values for π^0 mesons are found to be significantly above zero for the measured p_T range of 1–9 GeV/c. The v_4/v_2^2 ratios are independent of p_T with a magnitude between $\sim$0.8 and $\sim$1.0 depending on the centrality range, which may reflect the combined effects of fluctuations in the initial collision geometry and finite viscosity in the evolving medium.

ACKNOWLEDGMENTS

We thank the staff of the Collider-Accelerator and Physics Departments at Brookhaven National Laboratory and the staff of the other PHENIX participating institutions for their vital contributions. We acknowledge support from the Office of Nuclear Physics in the Office of Science of the Department of Energy, the National Science Foundation, Abilene Christian University Research Council, Research Foundation of SUNY, and Dean of the College of Arts and Sciences, Vanderbilt University (USA); Ministry of Education, Culture, Sports, Science, and Technology and the Japan Society for the Promotion of Science (Japan), Conselho Nacional de Desenvolvimento Científico e Tecnológico and Fundação de Amparo à Pesquisa do Estado de São Paulo (Brazil); Natural Science Foundation of China (P. R. China); Ministry of Education, Youth and Sports (Czech Republic); Centre National de la Recherche Scientifique, Commissariat à l'Énergie Atomique, and Institut National de Physique Nucléaire et de Physique des Particules (France); Bundesministerium für Bildung und Forschung, Deutscher Akademischer Austausch Dienst, and Alexander von Humboldt Stiftung (Germany); Hungarian National Science Fund, OTKA (Hungary); Department of Atomic Energy and Department of Science and Technology (India); Israel Science Foundation (Israel); National Research Foundation and WCU program of the Ministry Education Science and Technology (Korea); Physics Department, Lahore University of Management Sciences (Pakistan); Ministry of Education and Science, Russian Academy of Sciences, Federal Agency of Atomic Energy (Russia); VR and Wallenberg Foundation (Sweden); the US Civilian Research and Development Foundation for the Independent States of the Former Soviet Union, the US-Hungarian Fulbright Foundation for Educational Exchange, and the US-Israel Binational Science Foundation.

[1] K. Adcox *et al.* (PHENIX Collaboration), Nucl. Phys. A **757**, 184 (2005).
[2] J. Adams *et al.* (STAR Collaboration), Nucl. Phys. A **757**, 102 (2005).
[3] I. Arsene *et al.* (BRAHMS Collaboration), Nucl. Phys. A **757**, 1 (2005).
[4] B. B. Back *et al.* (PHENIX Collaboration), Nucl. Phys. A **757**, 28 (2005).
[5] B. Muller, J. Schukraft, and B. Wyslouch, Annu. Rev. Nucl. Part. Sci. **62**, 361 (2012).
[6] U. W. Heinz and P. F. Kolb, Nucl. Phys. A **702**, 269 (2002).
[7] M. Gyulassy, I. Vitev, and X. N. Wang, Phys. Rev. Lett. **86**, 2537 (2001).
[8] A. Adare *et al.* (PHENIX Collaboration), Phys. Rev. Lett. **98**, 172301 (2007).
[9] R. A. Lacey, N. N. Ajitanand, J. M. Alexander, P. Chung, W. G. Holzmann *et al.*, Phys. Rev. Lett. **98**, 092301 (2007).
[10] P. Romatschke and U. Romatschke, Phys. Rev. Lett. **99**, 172301 (2007).
[11] A. M. Poskanzer and S. A. Voloshin, Phys. Rev. C **58**, 1671 (1998).
[12] S. Afanasiev *et al.* (PHENIX Collaboration), Phys. Rev. C **80**, 024909 (2009).
[13] A. Adare *et al.* (PHENIX Collaboration), Phys. Rev. C **78**, 014901 (2008).
[14] J. Adams *et al.* (STAR Collaboration), Phys. Rev. Lett. **92**, 062301 (2004).
[15] A. Adare *et al.* (PHENIX Collaboration), Phys. Rev. Lett. **105**, 062301 (2010).
[16] G. Aad *et al.* (ATLAS Collaboration), Phys. Rev. C **86**, 014907 (2012).
[17] B. Abelev *et al.* (ALICE Collaboration), Phys. Lett. B **719**, 18 (2013).
[18] S. Chatrchyan *et al.* (CMS Collaboration), Phys. Rev. C **87**, 014902 (2013).
[19] J.-Y. Ollitrault, Phys. Rev. D **46**, 229 (1992).
[20] M. Gyulassy and X. N. Wang, Nucl. Phys. B **420**, 583 (1994).
[21] K. Adcox *et al.* (PHENIX Collaboration), Phys. Rev. Lett. **88**, 022301 (2002).

[22] A. Adare *et al.* (PHENIX Collaboration), Phys. Rev. Lett. **105**, 142301 (2010).
[23] A. Adare *et al.* (PHENIX Collaboration), Phys. Rev. C **87**, 034911 (2013).
[24] A. Adare *et al.* (PHENIX Collaboration), Phys. Rev. C **85**, 064914 (2012).
[25] S. S. Adler *et al.* (PHENIX Collaboration), Phys. Rev. Lett. **96**, 202301 (2006).
[26] R. A. Lacey, A. Taranenko, J. Jia, N. N. Ajitanand, and J. M. Alexander, arXiv:1105.3782.
[27] S. S. Adler (PHENIX Collaboration), Phys. Rev. C **69**, 034910 (2004).
[28] S. Afanasiev *et al.* (PHENIX Collaboration), Phys. Rev. C **80**, 054907 (2009).
[29] A. Adare *et al.* (PHENIX Collaboration), Phys. Rev. Lett. **107**, 172301 (2011).
[30] E. Richardson *et al.* (PHENIX Collaboration), Nucl. Instrum. Methods A **636**, 99 (2011).
[31] L. Aphecetche *et al.* (PHENIX Collaboration), Nucl. Instrum. Methods A **499**, 521 (2003).
[32] A. Adare *et al.* (PHENIX Collaboration), Phys. Rev. C **82**, 011902 (2010).
[33] N. Borghini and J. Y. Ollitrault, Phys. Rev. C **70**, 064905 (2004).
[34] B. I. Abelev *et al.* (STAR Collaboration), Phys. Rev. C **77**, 054901 (2008).
[35] S. Afanasiev *et al.* (PHENIX Collaboration), Phys. Rev. Lett. **99**, 052301 (2007).
[36] J. Jia (PHENIX Collaboration), Nucl. Phys. A **783**, 501 (2007).
[37] A. Adare *et al.* (PHENIX Collaboration), Phys. Rev. Lett. **101**, 232301 (2008).
[38] N. Borghini and J.-Y. Ollitrault, Phys. Lett. B **642**, 227 (2006).
[39] C. Gombeaud and J.-Y. Ollitrault, Phys. Rev. C **81**, 014901 (2010).
[40] J. Jia, Phys. Rev. C **87**, 061901(R) (2013).
[41] X. Zhang and J. Liao, Phys. Rev. C **87**, 044910 (2013).